Three-Dimensional Display of Positron Emission Tomography of the Heart

Tom R. Miller, Justin B. Starren, and Robert A. Grothe, Jr

The Edward Mallinckrodt Institute of Radiology, Washington University School of Medicine, St. Louis, Missouri

A method for producing images of ^{82}Rb myocardial perfusion and ^{11}C carbon monoxide gated blood pool images is described. In the case of ^{82}Rb images, cylindrical projection displaying myocardial activity as viewed from the side is presented to complement the polar projection. Cubic display of the conventional short- and long-axis slices is described that permits interactive selection of any desired slices. A three-dimensional cine display of the left ventricle rotating about its long axis is produced that gives a very realistic presentation of myocardial activity. Very similar processing techniques are applied to gated carbon-11 blood-pool studies to yield beating images of the surface of the blood pool in multiple projections.

J Nucl Med 29:530–537, 1988

The use of emission computed tomography for cardiac imaging with either thallium-201 (^{201}Tl) or positron-emitting radionuclides has increased greatly in recent years. Tomographic imaging is widely used in the analysis of myocardial perfusion (*1–4*), and tomographic data may be of value in assessing cardiac function with blood-pool agents (*5–7*). The utility of tomography is further enhanced by reconstruction of images in oblique orientations that are perpendicular (short axis) or parallel (long axis) to the major axis of the left ventricle (*1,4,8*). These oblique views lead to improved perception of perfusion abnormalities, especially those involving the posterior and inferior walls of the left ventricle. These tomographic reconstructions have the potential disadvantage of requiring the observer to integrate information from a very large number of images. Thus, there is great interest in display formats, such as the "bull's eye" polar projection (*9*) or cine-mode displays (*10*), that synthesize information from multiple views into a single image.

In this paper, we describe a new processing and display system for positron emission tomographic data incorporating numerous modifications to previously reported techniques.

Received Mar. 3, 1987; revision accepted Oct. 22, 1987.

For reprints contact: Tom R. Miller, MD, PhD, The Edward Mallinckrodt Institute of Radiology, 510 S. Kingshighway Blvd., St. Louis, MO 63110.

METHODS

Image Acquisition

The images shown here are obtained from positron emission tomography (PET) studies employing rubidium-82 (^{82}Rb), a myocardial perfusion agent (*11*), and carbon-11 (^{11}C) carbon monoxide, a blood-pool tracer (*12*). All studies were performed on the Super PETT I tomograph (*13*) which produces seven transaxial slices spaced 15 mm apart. Transaxial resolution employing a typical reconstruction filter is 15 mm full width half maximum (FWHM) and z-axis resolution is 11.4 mm FWHM. Transaxial slices are reconstructed in a 128 × 128 pixel format with pixel dimensions of 2.7 mm × 2.7 mm. Myocardial images of approximately 500,000 counts per slice were obtained during a constant intravenous infusion of ^{82}Rb from a strontium-rubidium generator. Blood-pool images were obtained following inhalation of [^{11}C] carbon monoxide. The gated blood-pool images were reconstructed from list mode data into eight frames per R-R interval.

Computer and Display Hardware

All computer processing and image manipulation of the transaxial slices was performed on a VAX-11/750 computer (Digital Equipment Corporation, Maynard, MA). Software was written in FORTRAN and Macro-11. Images were displayed on a video display system with eight image planes (256 colors or gray levels) and a 640 × 512 pixel image memory.

Image Reconstruction

Image processing is divided into two steps, parameter setting and batch-mode analysis. First, the user interactively assigns several parameters required for processing. The center of the heart and the angles defining the major axis of the heart

are determined from transaxial and rotated sagittal slices as described by others (*8*). Briefly, the operator first selects a transaxial slice through the midportion of the left ventricle and interactively positions a cursor and arrow to define the center of the ventricle and the long-axis of the ventricle in that transaxial plane. Then, after rotation of the data through the first angle, three sagittal images are displayed centered about the middle of the ventricle as defined in the first step. Now, a second cursor and arrow are positioned to specify the center of the heart in the axial (z) direction and to specify the second rotation angle. Finally, a short-axis slice is displayed to permit assignment of the third angle to align the septum vertically. After computation and display of the three-dimensional images, as described below, the center position and rotation angles can be reset more accurately, if necessary, by direct reference to the cubic data set during repositioning of the center point and long-axis vector.

In addition, the operator defines a region of interest containing the heart and a threshold activity value. In the myocardial perfusion studies, this threshold value is only used for background subtraction during display; the threshold setting does not play a role in edge detection. In the blood-pool images this threshold value is used for edge detection.

By separating parameter setting from the bulk of the computations, the initial processing steps require only approximately two minutes of operator time. The actual image processing is then done in batch mode without operator intervention. The batch mode computations require ~15 min on the VAX-11/750.

Image display and analysis is based on the construction of a 64 × 64 × 64 cubic data set (cuberille) with all three voxel dimensions having an equal length of 2.7 mm. First, the major axis of the heart is rotated to align with the z-axis of the cuberille using a three-angle back-projection algorithm. We choose to do a three-angle Euler rotation, rather than rotation through two-angles as used by others (*8-9*), because the three-angle rotation permits precise orientation of the interventricular septum. The first two rotations align the heart's major axis along the z-axis of the cuberille. The third rotation turns the heart about its long axis to precisely orient the interventricular septum vertically. In the ungated perfusion studies, the varying orientation of the long axis of the heart due to cardiac and respiratory motion cannot be determined. Thus, the long axis defined here represents the average orientation of the heart during the period of image collection.

Since the projected voxel following rotation will not usually align precisely with a voxel in the original transaxial data set, linear interpolation between the eight adjacent voxels of the original data is used to determine the activity in each voxel of the rotated cuberille (*14*). Because the entire transaxial image set can reside in memory in a VAX computer, it is possible to perform all three rotations simultaneously, rather than sequentially, as is required when using computers with more limited memory capacity. Furthermore, by performing a combined rotation only one interpolation step is required, thus increasing the accuracy of the interpolated image compared to that obtained when three sequential rotations and interpolations are required.

This obliquely-rotated 64 × 64 × 64 pixel cuberille represents the distribution of cardiac radioactivity in a form readily manipulated by the computer. As with the original transaxial data, the entire cubic array can reside in memory at one time, thus facilitating rapid determination of a true three-dimensional activity profile.

Myocardial Activity Profile

Computation of a myocardial activity profile is readily performed by processing the cuberille data in a spherical coordinate system (Fig. 1A). Each point P(X,Y,Z) in the cuberille can be expressed in terms of spherical coordinates (R,θ,ϕ), where R is the distance from the center of the left ventricle (X = Y = Z = 0) to the point of peak activity in the myocardial wall, θ is an angle between 0° and 180° such that the 0° vector points toward the base and the 180° vector points toward the apex, and ϕ is an angle between 0° and 360° rotating about the long axis of the heart with 0° pointing toward the lateral wall of the ventricle.

For each possible combination of θ and ϕ, a vector is projected outward from the center of the ventricle. The voxel with the greatest number of counts along a given vector is considered to represent the myocardial wall. In practice the angle θ is divided into 128 equal steps and ϕ is divided into 256 steps. The detected myocardial activity is then stored as a 2 × 128 × 256 array in computer memory with the first element for each θ and ϕ representing the peak activity along the vector and the second element the distance R from the center of the ventricle.

Bull's Eye and Cylindrical Projections

The spherical data set is easily converted into a bull's eye projection (Fig. 1B) in which the concentric rings of the bull's eye represent increments of the angle θ (from the base to the apex) with the angle ϕ running from 0° to 360° about the circumference of the ring.

Also generated is a cylindrical projection which is useful in identifying defects that are not in an apical location. This projection (Fig. 1C) is a rectangular display of the spherical-coordinate array described above containing the activity profile where, as with the bull's eye projection, the intensity at each point represents the myocardial activity. In producing these images it is not necessary to apply a smoothing filter to the data other than the smoothing inherent in the trilinear interpolation from the original transaxial images.

Interactive Display of Image Slices

Short- and long-axis images from the cuberille data set with the heart aligned along the z-axis of the cuberille are displayed using the interactive format shown in Figure 2. The cube shown in the upper left is used for orientation. The other three images are selected orthogonal views extracted from the cube representing the conventional short- and long-axis projections. These slices can be selected interactively with the new slice displayed in ~0.5 sec.

Three-Dimensional Cine Display

By converting the stored spherical-coordinate data back into Cartesian coordinates, a new cuberille can be constructed containing the entire three-dimensional profile of the myocardial pixels detected by the radial search described above. This process results in a three-dimensional array with values of zero at all locations except for the voxels comprising the peak activity profile. By searching inward from one face of this cube, the 'visible' voxels can be determined as the first non-

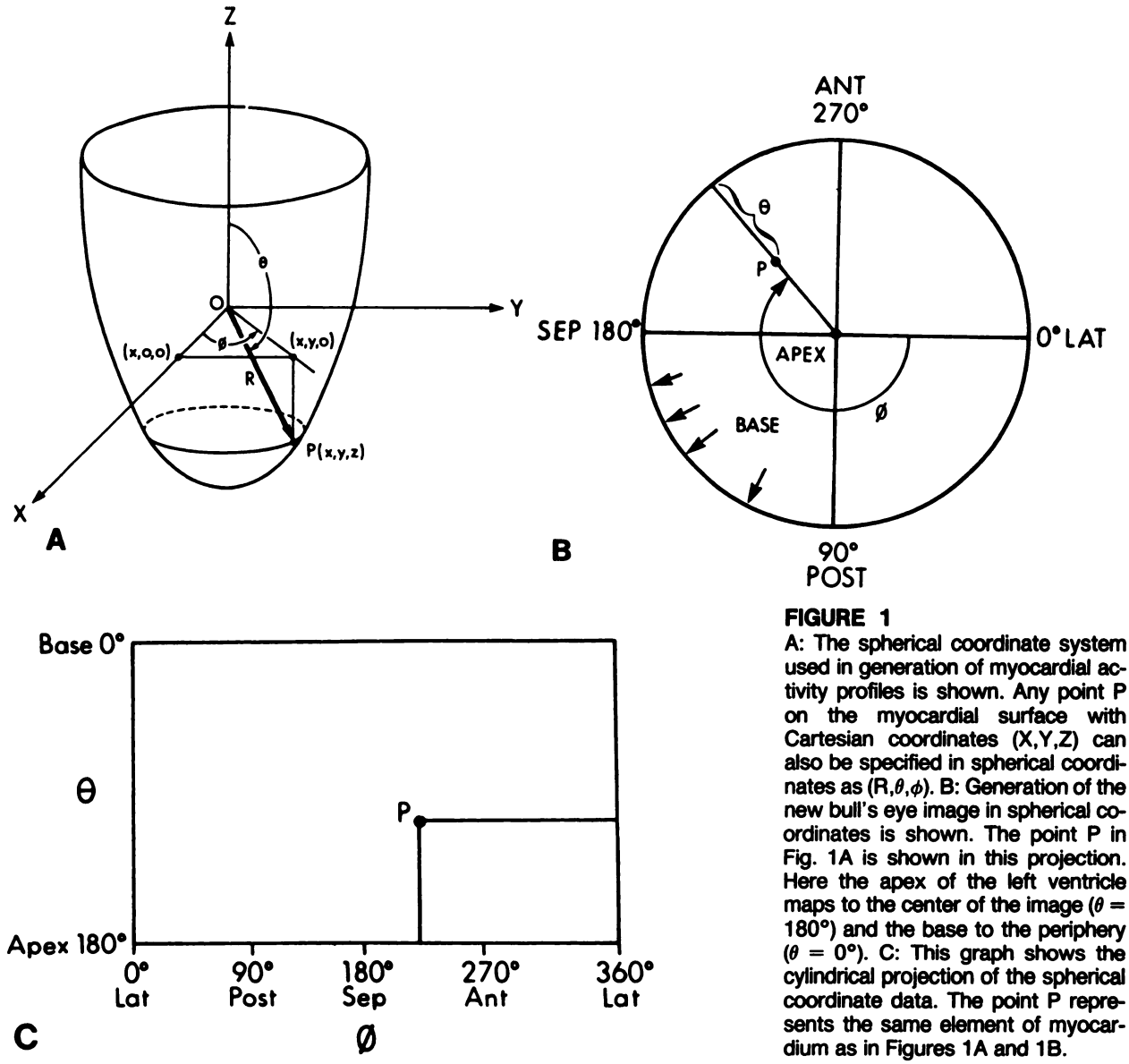

FIGURE 1
A: The spherical coordinate system used in generation of myocardial activity profiles is shown. Any point P on the myocardial surface with Cartesian coordinates (X,Y,Z) can also be specified in spherical coordinates as (R,θ,ϕ). B: Generation of the new bull's eye image in spherical coordinates is shown. The point P in Fig. 1A is shown in this projection. Here the apex of the left ventricle maps to the center of the image (θ = 180°) and the base to the periphery (θ = 0°). C: This graph shows the cylindrical projection of the spherical coordinate data. The point P represents the same element of myocardium as in Figures 1A and 1B.

zero array elements encountered (*15*). The counts in these voxels are then written into the corresponding pixels of a two-dimensional image array to be displayed. By rotating the cube a few degrees about its major axis and repeating the process, multiple images of the 'visible' activity surface can be generated. When displayed in an endless-loop cine, these images constitute a display of the myocardial activity viewed from the side as the heart rotates about its major axis.

To achieve a smoother margin in the rotating images, a conventional nine-point smoothing filter was applied to the two-dimensional array (R(θ,ϕ) containing the distance information. No smoothing of the array containing the radioactivity data was necessary. The mapping of the detected pixels, described in spherical coordinates, back into Cartesian coordinates was effected by a nearest-neighbor assignment. This process, of course, introduces additional smoothing, although of a small degree since the pixel dimensions are small.

For better visualization of apical defects, it is also possible to generate a set of cine images depicting the heart rotating end-over-end. This is easily done because the activity profile is stored in spherical coordinates. To rotate end-over-end, one need simply increment the angle θ between frames, rather than the angle ϕ as is done for rotation about the major axis.

Thresholding and Look-Through

The perception of perfusion defects in the cine display is often enhanced by removing voxels with subnormal activity and allowing the far wall of the heart to show through the defect. The user can interactively define a threshold for removal of voxels with abnormally low activity. The three-dimensional appearance of the image is further enhanced by including depth information in the displayed images. This is accomplished by generating a new cine display in which color indicates activity and brightness indicates depth (*16*). Because it is only necessary to differentiate near and far walls, only four depth levels (2 bits) are used in combination with 64 activity levels (6 bits). Since the 'visible" voxels are determined by searching in from the face of the cuberille, the depth parameter is readily available for computation of the depth level.

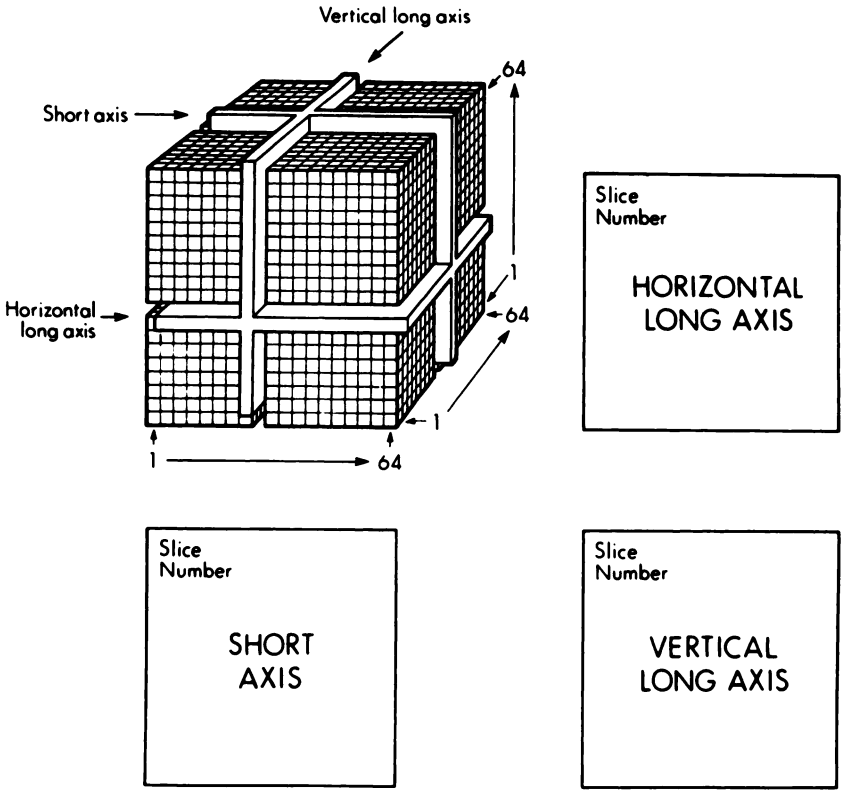

FIGURE 2
The 64 × 64× 64 pixel cuberille data set is shown with the major axis of the heart projecting out of the page. The user can quickly and interactively select any combination of short- and long-axis slices. The selected image data are extracted from the cuberille and displayed as shown.

Combined Cine-Mode Display

The bull's eye, cylindrical and cine displays described above can be displayed simultaneously, permitting rapid integration by the observer of all the three-dimensional information. In this display, moving indicator lines are added to the bull's eye and cylindrical projections to indicate the areas that correspond to the visible portion of the rotating surface projections.

Tomographic Blood-Pool Imaging

The algorithms described above are readily adapted to the analysis of gated blood-pool studies. For the PET study shown here, the gated blood-pool data consist of eight transaxial image sets, each 128 × 128 × 7 slices, spaced evenly throughout the cardiac cycle. Technetium-99m data would typically consist of 16–32 transaxial image sets, each 64 × 64 × 32 slices. First, center and orientation parameters are set by the operator for the end-diastolic images in the same way as described above for the myocardial studies. In addition to the parameters used for myocardial images, the operator also interactively defines separate regions of interest for each of the four chambers. The images are then processed in batch mode using the rotation parameters determined above, giving a total of 8 cuberilles, each 64 × 64 × 64 pixels in size, spanning the entire cardiac cycle. Images corresponding to short- and long-axis slices through the center of the ventricles are extracted and written to disc files for later display, giving cine images as previously described by others (*5–7*).

A new set of cine images are produced showing the surface of the cardiac blood pool. To determine the boundaries of the cardiac blood pool, all voxels in the cuberilles that are below a threshold level interactively determined by the operator are set to zero. A search is then performed inward from one of the six faces of each of the cuberilles to determine the depths of the first non-zero voxels. Those depths (not the activities of the voxels) are written into output arrays. Thus, the displayed images represent the surface of the cardiac blood-pool with intensity in the output images corresponding to distance from the viewer. This process is performed for all 8 or 16 cuberilles, and the output images are viewed in cine mode giving a beating image of the surface of the heart as seen from one direction. These computations are then repeated with inward searching from each of the other five faces of the cubes, thus leading to six sets of gated images of the cardiac blood-pool. The user has the option to add oblique lighting to the displayed images to enhance the three-dimensional effect (*17*). Total processing time is ~25 min on the VAX-11/750.

RESULTS

Figure 3 shows the rotated cuberille data derived from the transaxial images from a patient with a large anteroseptal myocardial infarction. Short- and long-axis slices demonstrating the perfusion defect have been selected interactively by the operator. Figure 4 shows the combined cine-mode display incorporating the bull's eye, cylindrical and three-dimensional cine images on a single display of a patient with a large lateral infarction. The upper right image is the rotating cine display without thresholding, while the lower right image incorporates the threshold removal so that the far wall of the ventricle shows through the "hole" produced by the infarction. The white lines on the static bull's eye and cylindrical images move in step with the rotation of the cine images. This combined display inte-

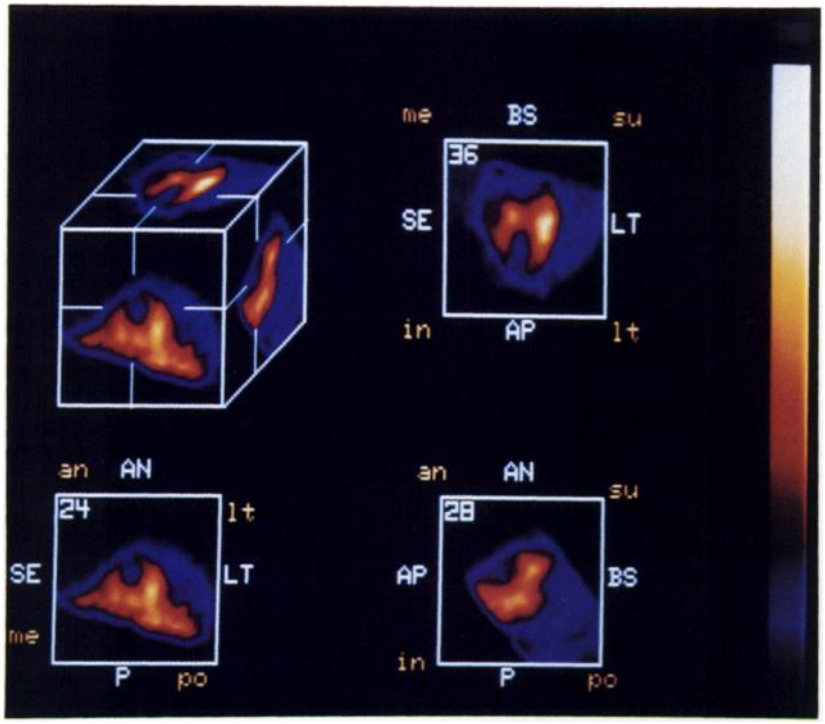

FIGURE 3
Rubidium-82 images of a patient show the interactive display of cuberille data with selected short- and long-axis slices specified by the index marks along the edges of the cube. The large white letters indicate the orientation of the heart in the rotated coordinate system while the smaller colored labels represent the orientation in relation to the patient's body. Note the large defect associated with anterior infarction (arrows).

grates essentially all the image information into a single, readily comprehended presentation.

Gated images of the surfaces of the cardiac blood pool in a normal subject obtained with [^{11}C]carbon monoxide are shown in Figure 5 with oblique lighting. End-diastolic images in anterior, right lateral, posterior, left lateral and apical projections are shown.

DISCUSSION

There are several key elements in our method for analysis of tomographic cardiac data that facilitate generation and display of a variety of useful images. The first element is the conversion of the initial transaxial images into a 64 × 64 × 64 pixel cube of data (cuberille)

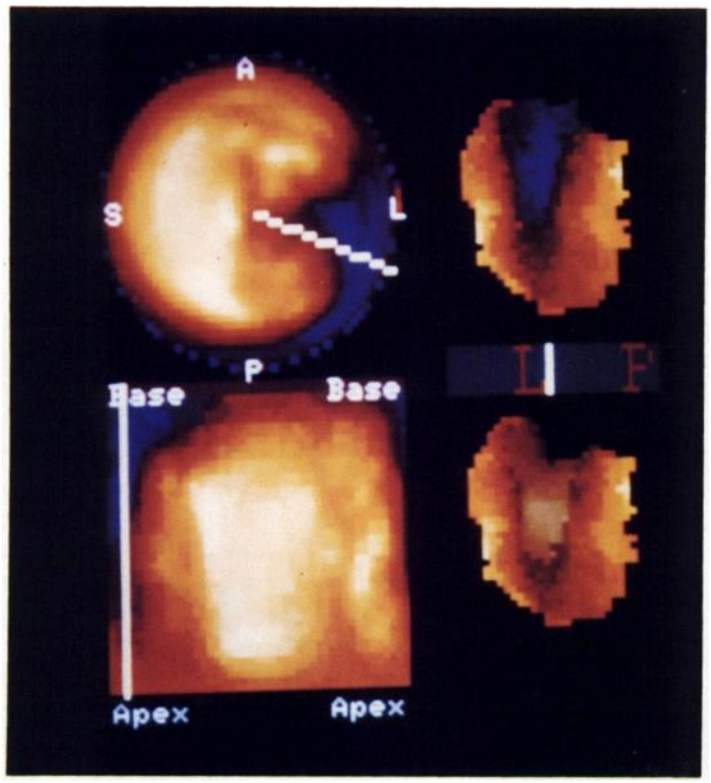

FIGURE 4
The combined cine-mode display of ^{82}Rb images is shown incorporating the bull's eye, cylindrical (left) and three-dimensional displays (right) shown separately in a patient with a large lateral infarct. The white lines on the bull's-eye and cylindrical displays move in step with the rotating three-dimensional display. Note the additional information in the three-dimensional displays and note that activity on the far wall of the ventricle is visualized in the lower image.

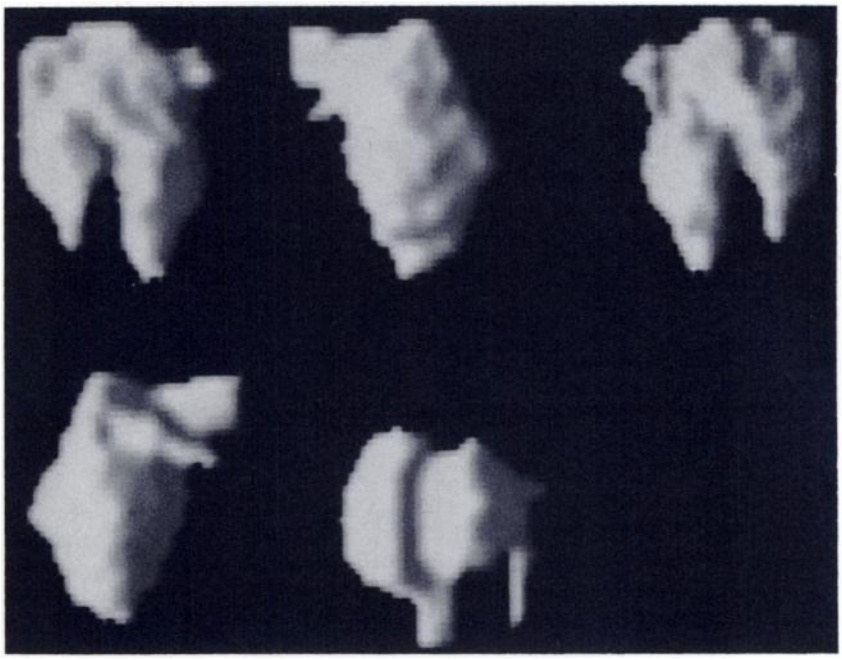

FIGURE 5
Gated blood-pool images from a normal subject are shown at end-diastole. Images in the upper row are in anterior, right lateral and posterior projections while the lower images are in left lateral and apical projections. To enhance the three-dimensional effect, oblique lighting has been applied.

oriented along the major axis of the heart (Fig. 2). The distribution of radioactivity in the heart is completely characterized by this cubic data set, permitting simple and efficient generation of various three-dimensional displays. Second, the ability readily to store and manipulate these arrays is critical to the improvements we have incorporated into this three-dimensional image processing system. Use of a 32-bit computer with virtual memory, such as the VAX or MicroVAX-II, greatly facilitates the manipulation of this large, three-dimensional data set. Prior to the availability of affordable 32-bit processors with large, inexpensive memory, cumbersome techniques were required to handle arrays as large as 64 × 64 × 64 pixels (*14*).

The conventional slice-wise method for determination of circumferential activity profiles in tomographic studies (*9*) has several fundamental limitations. Ideally, the search vector used to define myocardial activity should be perpendicular to the myocardial surface, thus minimizing the area of myocardium to be searched and improving the detection of small defects. Unfortunately, near the apex the short-axis slices and, therefore, the conventional search vectors, are roughly tangent to the myocardial surface. Some investigators have attempted to compensate for this problem by simply inserting apical activity, determined from long-axis slices, in the center of the bull's eye (*9*). While this approach gives some improvement, the transition from apical activity to circumferential activity often results in areas of overlap or gaps between the two determinations. This is especially evident when a perfusion defect involves the apex and extends to a lateral wall. Furthermore, since there are slices beyond the apex which contain no myocardium, the conventional approach requires the operator to select the slices to be included in the radial short-axis searches. This selection may be quite arbitrary, especially when apical defects are present.

We believe the heart can better be searched in a spherical coordinate system (Fig. 1A). Since the entire cuberille can be stored in computer memory at one time, it is possible to determine peak activity along any vector radiating from the center of the heart rather than limiting the search to individual short-axis slices. Since, in our method, all search vectors begin at the center of the left ventricle, the vectors are always approximately perpendicular to the myocardial surface. As a result, the apex is searched in the same manner as any other part of the ventricle, eliminating the requirement for special analysis of the apex. In hearts in which the walls run parallel to the long axis, the slice-wise approach may detect the wall in a more perpendicular fashion in a short segment. However, for most of the heart the radial search should be superior, and in dilated, spherical hearts the radial search will be superior for all segments.

Near the base of the heart (angle θ from ~0° to 30°) the search vectors do not transect ventricular wall. With our searching method this fact does not create a problem because the activity in the area of the atria and great vessels, although much lower than the ventricular activity, is still higher than in the tissues beyond. Thus, the search vectors will terminate in these structures. When the images are displayed these areas of low activity are easily distinguished from the regions of higher activity in the adjacent ventricular myocardium.

Other workers have constructed three-dimensional images of myocardial perfusion from slice-wise activity

profiles that are similar to our three-dimensional cine display (*10*). While these reconstructions give important information about the distribution of myocardial activity, they suffer from the same limitations at the apex and base as do the conventional bull's eye projections. Since our spherical activity profile represents the entire myocardium in a single data set, it is very easy to reconstruct a three-dimensional projection which avoids these limitations.

To further increase the usefulness of this three-dimensional display, we have included it in a combined cine-mode presentation (Fig. 4). In this display, the observer sees the bull's eye and cylindrical projections in addition to the original and threshholded three-dimensional images. The bull's eye and cylindrical displays are overlayed with moving guide lines to indicate the portion of the display corresponding to the visible portion of the three-dimensional image. Thus, essentially all the image information is available to the observer simultaneously in a readily comprehended form.

The interactive display of the oblique cuberille data (Figs. 2 and 3) provides ready access to a large number of views in a simplified, convenient format. Were all views to be displayed, the observer would be forced to contend with 192 separate images (3 × 64). Because the large VAX memory can store the entire 262,144 elements of the cuberille array at one time, it is possible to rapidly extract the desired slices from the cuberille and display them in less than one second. Thus, the observer has immediate access to all the short- and long-axis images with simultaneous display of the three intersecting orthogonal views of any portion of the heart. By including the orientation cube in the upper left corner of the display the observer always has a precise, graphic representation of the location of each slice, thus eliminating uncertainty about the relation among the various slices.

The use of tomographic blood-pool images has been advocated as a possible improvement over planar blood-pool imaging. Previously published work has centered on the interpretation of cine displays of reconstructed oblique slices through the cardiac chambers (5–7). The reconstruction of static blood-pool images of the surfaces of the cardiac chambers has been presented (*15*), but there has been little previous work (*18*) describing surface projections in gated cine-mode. We have added an additional feature to the surface reconstruction whereby the operator can define regions containing the four chambers, thus permitting display of any chamber or chambers as the heart rotates about its long axis. This display permits viewing of surfaces (such as the septal face) which would otherwise be hidden by other chambers.

Our PET data, with only seven slices, have inherently very coarse axial sampling. When this work began, we were concerned that acceptable three-dimensional images might have to await the acquisition of 14-slice studies from a newer PET machine. However, analysis of many seven-slice ^{82}Rb perfusion studies in patients with proven myocardial infarcts has failed to show any visually significant artifacts or undetected perfusion abnormalities. Thus, the trilinear interpolation algorithm, with its inherent smoothing properties, that we use to generate the cubic data set is more robust than expected. Single-photon studies yield many more transaxial slices, making the problem of axial sampling less important.

As described above, very little additional smoothing of the data was required to achieve visually acceptable three-dimensional images. We chose to retain a degree of noisiness in the images rather than introduce additional smoothing that would tend to degrade spatial resolution. In very low-count studies further smoothing could be added, if desired, at any one of several stages in the computations.

The images shown here are all from positron studies; no results with single-photon emitters are presented. However, the computational techniques for handling the positron and single-photon data are very similar. The principal differences are the closer slice spacing of the single-photon data that will greatly reduce the required interpolation, and the larger number of frames per R-R interval available in gated blood-pool studies employing ^{99m}Tc. However, qualitative image results with ^{201}Tl are expected to be similar to those reported here for ^{82}Rb since the total number of collected counts and the within-slice spatial resolution are similar. Our new three-dimensional display of gated blood-pool studies will also likely give useful images with ^{99m}Tc, since several other groups have successfully obtained three-dimensional images with ^{99m}Tc (*5–7,15,18*).

ACKNOWLEDGMENTS

The authors thank Drs. Mark A. Mintun and Jerold W. Wallis for helpful discussions, Linda Beck and Lorraine DiPlacido for their assistance in the preparation of the manuscript and Normal Hente and Thomas Murry for photography.

Supported in part by grant HL 17646, Specialized Centers of Research in Ischemic Heart Disease from the National Institutes of Health, Bethesda, Maryland.

REFERENCES

1. Ritchie JL, Williams DL, Harp G, et al. Transaxial tomography with thallium-201 for detecting remote myocardial infarction. *Am J Cardiol* 1982; 50:1236–1241.
2. Go RT, Cook SA, MacIntyre WJ, et al. Comparative accuracy of stress and redistribution thallium-201 cardiac single photon emission transaxial tomography and planar imaging in the diagnosis of myocardial ischemia [Abstract]. *J Nucl Med* 1982; 23:P25.

3. Prigent F, Friedman J, Maddhai J, et al. Comparison of rotational tomography with planar imaging for thallium-201 stress myocardial scintigraphy [Abstract]. *J Nucl Med* 1983; 24:P18.
4. Senda M, Yonekura Y, Tamaki N, et al. Interpolating scan and oblique-angle tomograms in myocardial PET using nitrogen-13 ammonia. *J Nucl Med* 1986; 27:1830–1836.
5. Gill JB, Moore RH, Tamaki N, et al. Multigated blood-pool tomography: new method for assessment of left ventricular function. *J Nucl Med* 1986; 27:1916–1924.
6. Tamaki N, Mukai T, Ishii Y, et al. Multiaxial tomography of heart chambers by gated blood-pool emission computed tomography using a rotating gamma camera. Radiology 1983; 147:547–554.
7. Underwood SR, Walton S, Ell PJ, et al. Gated blood-pool emission tomography: a new technique for the investigation of cardiac structure and function. *Eur J Nucl Med* 1985; 10:332–337.
8. Borrello JA, Clinthorne NH, Rogers WL, et al. Oblique-angle tomography: a restructuring algorithm for transaxial tomographic data. *J Nucl Med* 1981; 22:471–473.
9. Garcia EV, Van Train K, Maddahi J, et al. Quantification of rotational thallium-201 myocardial tomography. *J Nucl Med* 1985; 26:17–26.
10. Kehtarnavaz N, Philippe EA, DeFigueiredo RJP. A novel surface reconstruction and display method for cardiac PET imaging. *IEEE Trans Med Imag* 1984; MI-3:108–115.
11. Goldstein RA, Mullani NA, Wong W-H, et al. Positron imaging of myocardial infarction with rubidium-82. *J Nucl Med* 1986; 27:1824–1829.
12. Geltman EM, Biello DR, Welch MJ, et al. Characterization of nontransmural myocardial infarction by positron-emission tomography. *Circulation* 1982; 65:747–755.
13. Ter-Pogossian MM, Ficke DC, Yamamoto M, et al. Design characteristics and preliminary testing of Super Pett I, a positron emission tomography utilizing photon time-of-flight information (TOF PET). IEEE Trans Nucl Sci Supplement: Workshop on Time-of-Flight Tomography, May, 1982:37–41.
14. Herman GT, Liu HK. Display of three-dimensional information in computed tomography. *J Comput Assist Tomogr* 1977; 1:155–160.
15. Gibson CJ. Interactive display of three-dimensional radionuclide distributions. *Nucl Med Commun* 1986; 7:475–487.
16. Goldman KJ, Miller TR. Interactive combining of functional images. *Eur J Nucl Med* 1985; 11:221–223.
17. Foley JD, VanDam A. Fundamentals of interactive computer graphics. Reading, MA: Addison-Wesley Publishing Co., 1982:575–591.
18. Faber TL, Stokely EM, Willerson JT, et al. A method for 3-D analysis and display of gated blood pool tomograms [Abstract]. *J Nucl Med* 1986; 27:918.